1 **Dating the termination of the Palaeoproterozoic Lomagundi-Jatuli carbon isotopic**

2 **Event in the North Transfennoscandian Greenstone Belt**

3

4 A. P. Martin[1*], D. J. Condon[1], A. R. Prave[2], V. A. Melezhik[3, 4], A. Lepland[3, 5], A. E. Fallick[6]

5

6

7 **1** NERC Isotope Geosciences Laboratory, British Geological Survey, Keyworth, NG125GG, UK

8 **2** Department of Earth Sciences, University of St Andrews, St Andrews, Scotland, UK

9 **3** Geological Survey of Norway, Postboks 6315 Slupen, 7491 Trondheim, Norway

10 **4** Centre for Geobiology, University of Bergen, Postboks 7803, N-5020 Bergen, Norway

11 **5** Tallinn Technical University, Institute of Geology, 19086 Tallinn, Estonia

12 **6** Scottish Universities Environmental Research Centre, East Kilbride, Glasgow G75 0QF, Scotland.

13 *adam@bgs.ac.uk

14

15 **Abstract**

16 **Existing radio-isotopic age constraints indicate that the global Palaeoproterozoic**
17 **Lomagundi-Jatuli large, positive carbonate carbon isotopic excursion, with δ^{13}C values**
18 **> +5‰, occurred between 2.2 and 2.06 Ga. In the North Transfennoscandian**
19 **Greenstone Belt of the Kola Peninsula, NW Russia, northern Norway and Finland, the**
20 **Lomagundi-Jatuli Event is recorded in the carbonate rocks of the Umba and Kuetsjärvi**
21 **Sedimentary formations in the Imandra-Varzuga and Pechenga greenstone belts. In**
22 **both areas, thick mafic volcanic units (Umba and Kuetsjärvi Volcanic formations)**
23 **overlie the sedimentary units recording the excursion. Overlying younger sedimentary**
24 **units contain carbonate rocks with δ^{13}C values typically ranging between c. -1 and +3‰,**
25 **signalling the termination of the Lomagundi-Jatuli excursion.**

26 **Two new U-Pb ID-TIMS (isotope-dilution thermal ionisation mass spectrometry) zircon**
27 **dates constrain this termination in both successions. The lower unit of the Il'mozero**
28 **Sedimentary Formation is a cross- and parallel-bedded volcaniclastic greywacke**
29 **derived largely from erosion of the underlying Umba Volcanic Formation. It has yielded**
30 **detrital zircons with ^{207}Pb/^{206}Pb dates as young as 2055.5 ± 2.3 Ma, which is a maximum**
31 **age for deposition and is inferred to date part of the underlying Umba volcanics. In**
32 **Pechenga, the Kolosjoki Sedimentary Formation was intersected by a drill hole**
33 **obtained by the ICDP (International Continental Scientific Drilling Program) -**
34 **supported FAR-DEEP (Fennoscandian Arctic Russia - Drilling Early Earth Project)**
35 **drilling programme. Zircons from a mafic fine tuff in this drill core have yielded a**
36 **^{207}Pb/^{206}Pb age of 2056.6 ± 0.8 Ma. This age is interpreted as an eruption age**
37 **contemporaneous with sedimentation. The new age determinations overlap each other**
38 **within uncertainty, and is within error of previously published detrital zircon ages of**
39 **2058 ± 2 Ma from the Kolosjoki Sedimentary Formation and 2049 ± 28 Ma from the**
40 **Kuetsjärvi Volcanic Formation. Combined, these indicate that the Lomagundi-Jatuli**
41 **excursion terminated across Fennoscandia by 2056.6 ± 0.8 Ma and may correlate with**
42 **similar termination ages in Fennoscandia and the Transvaal, South Africa.**

43

1. Introduction

The early Proterozoic records Earth's transformation from an anoxic to an oxygenated planet and is characterised by intervals of global rifting, termination of major banded iron formation, appearance of red beds, and perturbations in the cycles and accumulation of sulphur, phosphate, and carbon. Among these perturbations, one of the largest known positive carbonate carbon isotope excursions, termed the Lomagundi-Jatuli Event (Melezhik et al., 2005), is unique in Earth history. During the Lomagundi-Jatuli Event δ^{13}C values of +10-15‰ V-PDB (Vienna Pee Dee Belemnite; all δ^{13}C values are relative to V-PDB hereafter) were not uncommon. Values of δ^{13}C of 0 ± 5‰ in marine carbonate rocks are typical throughout geological time (Shields and Veizer, 2002) and are considered to reflect a balance between organic and inorganic carbon pools at a ratio of approximately 1:4 (the Ronov ratio; Aharon, 2005). Positive excursions away from these *normal* near zero values are interpreted as either due to increased organic carbon productivity and burial, or reduced carbonate deposition. Thus carbon isotope excursions are proxies for large-scale transformations in the carbon cycle, possibly related to varying atmospheric-oceanic conditions, tectonic regimes, and biospheric evolution.

The origin of the name for the Lomagundi-Jatuli Event comes from the eponymous regions in Zimbabwe and Fennoscandia where strongly positive δ^{13}C values in Proterozoic carbonate rocks were first reported (Galimov et al., 1968; Schidlowski et al., 1975, 1976). Baker and Fallick (1989) suggested this excursion was global in nature and it has now been recognised on all continents except Antarctica. Karhu (1993), based on data from Fennoscandia, and Karhu and Holland (1996), who compiled all of the then existing radiometric ages, proposed that the Lomagundi-Jatuli Event occurred between 2.22 and 2.06 Ga. However, radiometric dates that can constrain tightly the initiation, duration, or termination of the excursion are few (see Melezhik et al., 2012b, for a recent review).

Here, we report two new, high precision U-Pb ID-TIMS (isotope dilution thermal ionisation mass spectrometry) zircon radiometric dates determined on samples obtained by a recent

76   ICDP (International Continental Scientific Drilling Program) -sponsored project, FAR-DEEP

77   (Fennoscandian Arctic Russia - Drilling Early Earth Project; see http://www.icdp-online.org

78   for details) in the Russian sector of Fennoscandia. These provide the first age constraint on

79   the Lomagundi-Jatuli Event in the Imandra-Varzuga belt and further constrain its timing in

80   Pechenga.

81

2. Geological Setting

83   Palaeoproterozoic supracrustal units in northern Fennoscandia crop out discontinuously over

84   ~1000 km across the Kola Peninsula of NW Russia and from there into northern Norway and

85   Finland (Fig. 1). They rest unconformably on Archaean rocks and are preserved in segments

86   known as the Ust'ponoy, Imandra-Varzuga, Pechenga, Pasvik, Opukasjärvi, and Polmak

87   Greenstone Belts (Fig. 1; Melezhik and Sturt, 1994). Collectively, these are termed the North

88   Transfennoscandian Greenstone Belt. The best studied segment is Pechenga (Fig. 2), which

89   hosts world-class nickel-sulphide deposits (Alapieti and Lahtinen, 2002), and is the site of the

90   Kola Superdeep Drill Hole (Kozlovsky, 1987). The most aerially extensive segment is

91   Imandra-Varzuga (Fig. 3), which extends for more than 350 km along strike. Sedimentary

92   successions in both regions were the focus of FAR-DEEP, which recovered fresh diamond

93   drill cores as well as samples from outcrop (Melezhik et al., 2012a).

94

95   *2.1 Pechenga*

96   The Pechenga supracrustal succession sits unconformably on Archaean basement and

97   comprises the North and South Pechenga Groups. The former is composed of several

98   alternating thinner sedimentary (1500 m total), and thicker volcanic formations (6500 m total;

99   Melezhik and Sturt, 1994). The basal unit is the Neverskrukk Formation, consisting of

100   polymict conglomerates and immature sandstones containing clastic material derived from

101   the underlying basement complex (Fig. 2, 4). Above this are the mafic to intermediate lava

102   flows and intrusive rocks of the Amahlati Formation that, in turn, are overlain by the

103   Kuetsjärvi Sedimentary Formation. It is in this latter unit, consisting of red-coloured

104   sandstone and carbonate rocks, including stromatolitic carbonates, that the Lomagundi-Jatuli

105   excursion is recorded, with $\delta^{13}C$ values $\leq +9‰$ (Melezhik et al., 2007). The sedimentary units

106   are overlain by mafic to felsic alkaline volcanic rocks with subordinate volcaniclastic

107   conglomerates of the Kuetsjärvi Volcanic Formation. In sharp contact on those igneous rocks

108   is the Kolosjoki Sedimentary Formation, marked by basal volcaniclastic and arkosic

109   sandstones and then a succession of finer sandstones, dolomitic carbonates and minor tuffs;

110   the carbonate rocks have $\delta^{13}C$ values mostly between $+1 \leq \delta^{13}C$ ‰ $\leq +2.5$ (Melezhik et al.,

111   2007). The overlying Kolosjoki Volcanic Formation is tholeiitic basalts and mafic tuffs with

112   subordinate ferropicritic extrusive rocks and is overlain by the Pilgujärvi Sedimentary

113   Formation. The latter consists of carbonaceous- and sulfide-rich turbidite sandstones, fine-

114   grained siliciclastic rocks, and minor, mafic and ferropicritic tuffs and lavas at the top of the

115   formation. The Pilgujärvi Sedimentary Formation also contains several economic, ultramafic-

116   hosted, sulphide, Ni-Cu deposits. The topmost unit of the North Pechenga Group is the

117   Pilgujärvi Volcanic Formation consisting of pillowed and massive tholeiitic lava flows and

118   subordinate ferro-picrite flows and felsic tuffs. More detailed descriptions of Pechenga

119   geology are in Melezhik and Sturt (1994), Sharkov and Smolkin (1997), and references

120   therein.

121

122   *2.2 Imandra-Varzuga*

123   The lowermost rocks of the Imandra-Varzuga supracrustal succession are tholeiitic basalts

124   and polymict sandstones of the Purnach Formation and overlying Kuksha Sedimentary

125   (arkosic sandstone, greywacke, conglomerate) and Volcanic (tholeiitic basalt) formations that

126   sit unconformably on Archaean basement (Fig. 3, 4). The succeeding Seidorechka

127   Sedimentary Formation consists mostly of flaser-bedded greywacke-shale, cross-bedded and

128   rippled quartzitic sandstones, parallel-bedded siltstones and a thin dolostone that has $\delta^{13}C$

129   values between -1.8 and +3.5‰ (Melezhik and Fallick, 1996). These rocks are overlain by

130   komatiitic-basaltic lava flows and tuffs of the Seidorechka Volcanic Formation and by the

131   inferred Huronian-equivalent glacial deposits of the Polisarka Sedimentary Formation, with

132   siltstone and sandstone beds including dropstones and polymict conglomerates. The glacial

133   rocks are then overlain by spinifex-textured lava flows, volcanic breccias, and intermediate

134   lava flows that comprise the Polisarka Volcanic Formation. The Umba sedimentary-volcanic

135   couplet occurs above those lavas and consists of red-coloured, cross-bedded sandstones,

136   siltstones, and dolostones overlain by mafic and intermediate alkaline lava flows and

137   subordinate picrites. The Umba dolostones are interpreted as recording the Lomagundi-Jatuli

138   excursion with $\delta^{13}C$ values $\leq +6.7$‰ (Melezhik and Fallick, 1996). Resting erosionally on the

139   Umba volcanic rocks is the Il'mozero Sedimentary Formation, which consists of cross- and

140   parallel-bedded volcaniclastic greywacke and siltstones, black shales, dolostones, and

141 stromatolitic dolostones having $\delta^{13}C$ values from -0.8 to +2.4‰ (Melezhik and Fallick,

142 1996). Tholeiitic lava flows, tuffs, and lava breccias of the Il'mozero Volcanic Formation

143 overlie these sedimentary units. See Melezhik and Sturt (1994) and Sharkov and Smolkin

144 (1997) for further geological descriptions.

145

146 2.3 *Existing Chronology*

147 In Pechenga, the Archaean basement is cross-cut by the General'skaya gabbro-norite

148 intrusion dated by $^{207}Pb/^{206}Pb$ ID-TIMS (zircon) at 2505 ± 1.6 Ma (Amelin et al., 1995),

149 providing a maximum age for the supracrustal rocks (Fig. 4). The middle part of the

150 Kuetsjärvi Volcanic Formation and the base of the Kolosjoki Sedimentary Formation consist

151 of volcaniclastic conglomerates and greywackes sourced from the Kuetsjärvi Volcanic

152 Formation, from which detrital zircons have been recovered and dated by $^{207}Pb/^{206}Pb$ ID-

153 TIMS at 2058 ± 2 Ma (Melezhik et al., 2007), and as such provides a maximum age for the

154 stratigraphic level sampled within the Kolosjoki Sedimentary Formation. Melezhik et al.

155 (2007) argued for the underlying volcanic rocks being the only probable source of the

156 youngest detrital zircons in the Kolosjoki Sedimentary Formation and thus infer a c. 2058 Ma

157 age for part of the Kuetsjärvi Volcanic Formation (Fig. 4). A minimum age has been

158 determined on detrital zircons in the Kuetsjärvi Volcanic Formation at 2049 ± 28 Ma in

159 volcaniclastic conglomerates which crop out with an erosional contact on the irregular

160 palaeosurface of alkaline felsic lava breccias in the middle of the formation (Melezhik et al.,

161 2007; Fig. 4). A felsic volcanic unit in the Pilgujärvi Volcanic Formation (Fig. 4) has yielded

162 an ID-TIMS $^{207}Pb/^{206}Pb$ zircon age at 1970 ± 5 Ma (Hanski et al., 1990). The lower Kuksha

163 Volcanic Formation in Imandra-Varzuga is intruded by the Monche Pluton and the Pana

164 Tundra Intrusion, dated by U-Pb ID-TIMS (zircon) at 2504.4 ± 1.5 and 2501.5 ± 1.7 Ma

165 (Amelin et al., 1995), providing a minimum age constraint for the Kuksha Volcanic

166 Formation (Fig. 4). Magmatic bodies interpreted as feeder dykes and intrusions related to the

167 Seidorechka Volcanic Formation yield $^{207}Pb/^{206}Pb$ dates of 2442.2 ± 1.7 Ma (baddeleyite) on

168 a sub-volcanic unit and 2441 ± 1.6 Ma (zircon) on the spatially associated Imandra lopolith

169 (both by U-Pb ID-TIMS; Amelin et al., 1995; Fig. 4).

170

171 **3. Sample Descriptions**

172   In order to better constrain the timing of the Lomagundi-Jatuli excursion, the Il'mozero

173   Sedimentary Formation in Imandra-Varzuga, and the Kolosjoki Sedimentary Formation in

174   Pechenga, were sampled for U-Pb dating. Sample Il'mozero 1 was collected from outcrop

175   (67°06'45.0" N, 035°41'23.5" E; Fig. 3) in the lowermost Il'mozero Sedimentary Formation.

176   It yielded zircons that were analysed by laser ablation inductively coupled plasma mass

177   spectrometry (LA-ICPMS) and by ID-TIMS. Sample 8B 151.42m is from the Kolosjoki

178   Sedimentary Formation and was obtained from diamond drill core of Hole 8B of FAR-DEEP

179   in the Pechenga belt. It yielded zircons that were dated by the ID-TIMS method.

180

181   *3.1 Sample Il'mozero 1 (Imandra-Varzuga)*

182   In outcrop the Il'mozero Sedimentary Formation sits unconformably on the Umba Volcanic

183   Formation (Fig. 2, 4). Sample Il'mozero 1 is part of an interbedded succession of thin-bedded

184   sandstone and shale that occurs approximately 50 m above the contact with the underlying

185   Umba lava flows; the rocks are at lower greenschist facies. In hand specimen, it is a fine-

186   grained greywacke that exhibits grading and cm-scale layering. Cleavage is well-developed

187   and at a high angle to bedding. The middle part of the Il'mozero Sedimentary Formation (c.

188   30-40 m above the stratigraphic horizon of sample Il'mozero 1) is marked by 10 m of

189   interbedded shale and light grey dolostones that record normal $\delta^{13}C$ values (Melezhik and

190   Fallick, 1996). In thin section bedding is defined by a change in grain size from c. 80 μm to

191   50 μm, with well-sorted, poorly rounded grains (Fig. 5a; S1a). Quartz is the most common

192   mineral: pyroxene and plagioclase are minor at 1-2 volume percent (visual estimation; Fig.

193   S1b, c). The pyroxene is euhedral and acicular, ≤ 300 μm long, with 87° cleavage, is

194   pleochroic on the [100] face (α) from green to green-yellow and displays second-order

195   birefringence, optical properties that are consistent with augite. These primary grains are

196   overprinted by chlorite and pyrite. Augite and plagioclase are key mafic rock minerals that

197   break-down quickly in the sedimentary environment; their presence suggests a proximal,

198   (ultra-) mafic igneous source, presumably the underlying Umba Volcanic Formation. The

199   morphology of the zircons recovered from sample Il'mozero 1 was variable between

200   elongated, clear grains ≤ 200 μm in size with medial melt inclusion traces and sub-rounded,

201   equant grains ≤ 100 μm in size (Fig. S2). Cathode luminescence images show growth zoning

202   typical of magmatic crystals, with rare rims on the equant grains (Fig. S2).

203

204   *3.2 Sample 8B 151.42m (Pechenga)*

205   Sample 8B 151.42m is derived from the 336 m long FAR-DEEP drillcore 8B (69°27'56''N,

206   30°32'08'' E; Fig. 2) that intersects the Kolosjoki Sedimentary Formation. The base of the

207   Kolosjoki Sedimentary Formation occurs at c. 322 m in the drill core where the first

208   sandstone bed that sits on rocks inferred to be intermediate volcanic lava flows and tuffs.

209   Above this, the remaining 322 m consist mostly of sandstone units with minor greywacke and

210   carbonate layers. The core interval 90 to 190 m is characterised by elevated chromium and

211   nickel concentrations and is interpreted to be composed largely of ultramafic tuffs (Melezhik

212   et al., 2012c).

213

214   In hand specimen, fragments of crystals and scoria (c. 500 μm) have a common alignment,

215   giving the rock a discontinuous, streaky appearance (Fig. 5b). The sampled unit is 6 cm thick,

216   melanocratic, and exhibits a sharp upper and lower contact in hand specimen. In thin section

217   the lower contact (the upper contact is not visible in the thin section) is sharp; below the

218   contact scoria and crystal fragments (500 μm) are absent (Fig. S1d). There is a bi-modal size

219   distribution (Fig. S1e, f), with larger (500 μm) scoria clasts and plagioclase crystals

220   supported by finer-grained crystals (20 μm). Many of the plagioclase crystals have been

221   pseudomorphed by pyrite. There is also extensive carbonate alteration (Fig. S1e) from the

222   breakdown of volcanic glass. Scoria clasts are elongate, with rough and ragged edges, and a

223   near uniform size of 500 μm on the long axis (Fig. S1f). The fragments and crystals are not

224   commonly found as epiclasts (Boggs, 2010; Pettijohn et al., 1987), and given their rough

225   edges and common angularity (Fig. S1e, f), indicate little or no re-working, consistent with

226   the absence of sedimentary features. These characteristics suggest that sample 8B 151.42m is

227   a primary igneous deposit, with the scoria and larger crystals part of a porphyritic texture in a

228   fine-grained groundmass. The preservation of plagioclase, and the melanocratic colour index

229   indicate a mafic composition and the rock is best interpreted as a mafic fine tuff

230   (classification after White and Houghton, 2006), subsequently altered to lower greenschist

231   facies. Zircon crystals (20 – 70 μm; Fig. S2) were extracted from a 6-cm-long (1/4 core)

232   sample between 151.42 m and 151.48 m in FAR-DEEP drill core 8B.

233

234   **4. Methods**

235   Zircons were analysed using a combined LA-ICPMS and ID-TIMS methodology at the

236   NERC Isotope Geoscience Laboratory (NIGL), Keyworth, U.K. The LA-ICPMS method

237   yields radiometric dates on the detrital zircon population in sample Il'mozero 1, and provide

238   a means to identify suitable chronology targets prior to dissolution for ID-TIMS analysis. All

239   zircons were subject to a modified chemical abrasion pre-treatment for the elimination of Pb-

240   loss (Mattinson, 2005). The $^{207}Pb/^{206}Pb$ dates are based upon the dual decay of ^{238}U to ^{206}Pb

241   and ^{235}U to ^{207}Pb, and their accuracy is controlled by the precision and accuracy of the

242   radiogenic $^{207}Pb/^{206}Pb$ ratio, the present-day $^{238}U/^{235}U$ ratio, and the decay constants of ^{235}U

243   and ^{238}U (see section 4.1 and online supplemental material for details and further discussion).

244   In order to obviate any issues related to non-zero age Pb-loss and compromised $^{207}Pb/^{206}Pb$

245   dates we place an emphasis on zircon U-Pb data that are concordant at the high-level of

246   precision afforded by the ID-TIMS method. For carbonate stable isotope analysis, 1 mg

247   samples were dissolved overnight in phosphoric acid at 70° C. Isotope ratios were measured

248   at the Scottish Universities Environment Research Council on PRISM III and AP2003 mass

249   spectrometers. Repeat analyses of NBS-18 and internal calcite standards are generally better

250   than ± 0.2‰.

251

252   4.1 *Comment on dating methods and uncertainties*

253   In this contribution published radio-isotopic dates are combined with new data and this

254   requires consideration of systematic uncertainties associated with these dates. Firstly, when

255   comparing dates derived from different isotopic decay schemes the systematic uncertainty

256   related to the decay constant value must be considered (see Condon and Bowring, 2011, for a

257   recent review). However, when assessing the relative ages of samples dated using the same

258   decay scheme, it is sufficient to consider only uncertainty derived from non-systematic

259   sources. Secondly, recent studies have suggested that the natural $^{238}U/^{235}U$ ratio should no

260   longer be considered invariant and is not equal to 137.88 (Condon et al., 2010; Hiess et al.,

261   2012; Stirling et al., 2007), and a value of 137.818 ± 0.045 has been suggested for use in U-

262   Pb zircon geochronology (Hiess et al., 2012). Using this more accurate value with its

263   associated uncertainty has the effect of lowering $^{207}Pb/^{206}Pb$ dates at c. 2 Ga by 0.8 ± 0.6

264   Myr. In this study, $^{207}Pb/^{206}Pb$ dates cited have been determined using a $^{238}U/^{235}U$ value equal

265   to 137.88. In Table S1 (online summary table) we list the interpreted dates for the samples of

266   interest calculated using both $^{238}U/^{235}U$ = 137.88 and 137.818 ± 0.045.

267

268   **5. Results**

269   *5.1 U-Pb*

270   5.1.1 Sample Il'mozero 1

271   *LA-ICPMS:* Results less than 5% discordant are included on a relative probability plot of

272   ^{207}Pb/^{206}Pb ages from LA-ICPMS data in Fig. S3. Over 50% of the ^{207}Pb/^{206}Pb ages are

273   between 2100 and 2000 Ma, with a concentration of ages between c. 2080 and 2060 Ma

274   (Table 1). The youngest ^{207}Pb/^{206}Pb age in this range is 2063 ± 9 Ma (1.4% discordant).

275   Grains in the age range 2080 to 2060 Ma have magmatic growth zoning and equant

276   morphology (Fig. S2) and grains with this morphology were subsequently targeted for ID-

277   TIMS analysis.

278   *ID-TIMS:* Seven single zircon crystals were analysed by ID-TIMS (Table 2). One grain (z1)

279   is slightly discordant (Fig. 6a), indicating minor Pb-loss. The ^{207}Pb/^{206}Pb dates for the six

280   other grains (z2, z4 - 6, z9, z12) overlap within uncertainty (Fig. 6b), with z9 yielding the

281   youngest ^{207}Pb/^{206}Pb date at 2055.5 ± 2.3 Ma. A second grain (z12) yielding a ^{207}Pb/^{206}Pb

282   date of 2055.67 ± 2.3 Ma, gives confidence that youngest zircon (z9) has not experienced any

283   minor Pb-loss and is an appropriate youngest age. Incorporation of the uncertainties in λ^{235}U

284   and λ^{238}U (Jaffey et al., 1971) increases the uncertainty to 2.4 Myr. The ages yielded from the

285   youngest zircon grains by ID-TIMS and LA-ICPMS overlap within uncertainty. Based upon

286   the concordant U-Pb systematics and the morphology of the dated zircons, the ^{207}Pb/^{206}Pb

287   date of 2055.5 ± 2.3/2.4 Ma (analytical/total uncertainty) is interpreted to reflect the

288   maximum age of sample Il'mozero 1 and therefore the Il'mozero Sedimentary Formation at

289   this stratigraphic level.

290

291   5.1.2 Sample 8B 151.42m

292   *ID-TIMS:* Seven single zircon crystals were analysed by ID-TIMS (Table 2) yielding

293   concordant data (Fig. 6a) and ^{207}Pb/^{206}Pb dates between 2053.7 ± 4.7 and 2057.6 ± 2.3 Ma,

294   which overlap within uncertainty (Fig. 6b) and yield an error weighted mean ^{207}Pb/^{206}Pb date

295   of 2056.6 ± 0.8 Ma (n = 7, MSWD = 0.89); this implies that the seven zircons are equivalent

296   in age. Incorporation of the uncertainties in λ^{235}U and λ^{238}U (Jaffey et al., 1971) increases the

297   uncertainty to 0.9 Myr. Based upon the concordant U-Pb systematic and the morphology of

298   the dated zircons the ^{207}Pb/^{206}Pb date of 2056.6 ± 0.8/0.9 Ma (analytical/total uncertainty) is

299   interpreted to reflect the age of the mafic fine tuff and the age of the sampled stratigraphic

300   level.

301

302   *5.2 Stable isotopes*

303   Carbon and oxygen isotope data measured on carbonate samples from the Il'mozero

304   Sedimentary Formation are shown in Table 3. The $\delta^{13}C$ values range from a minimum of -

305   0.7‰ to a maximum of +2.6‰ and the $\delta^{18}O$ values vary between -13.8 and -9.3‰ (relative

306   to Vienna Standard Mean Ocean Water: V-SMOW). The carbonate samples overlie by c. 10

307   m the dated sample Il'mozero 1.

308

309   **6. Discussion**

310   The 2055.5 ± 2.3 Ma age obtained from detrital zircons in the Il'mozero Sedimentary

311   Formation is the first robust age from the upper part of the Imandra-Varzuga succession. The

312   proximity of carbonates with normal $\delta^{13}C$ values above the dated interval, and the underlying

313    $\delta^{13}C$ values up to +6.7‰, indicate that 2055.5 ± 2.3 Ma constrains the tail end, or

314   termination, of the Lomagundi-Jatuli Event in this part of the North Transfennoscandian

315   Greenstone Belt. The 2055.5 ± 2.3 Ma age from Imandra-Varzuga is a maximum age for the

316   Il'mozero Sedimentary Formation at this stratigraphic level. However, based upon the

317   stratigraphic relationship of the dated Il'mozero 1 sample overlying the Umba Volcanic

318   Formation, and petrography, it is inferred that the 2055.5 ± 2.3 Ma also dates part of the

319   Umba Volcanic Formation volcanic rocks and approximates the timing of sediment

320   accumulation/volcanism at this broad stratigraphic level. A similar argument is presented in

321   Melezhik et al. (2007), where zircon dated at 2058 ± 2 Ma in volcaniclastic-rich sediments in

322   the Kolosjoki Sedimentary Formation, Pechenga, is interpreted to date the underlying

323   Kuetsjärvi Volcanic Formation.

324

325   The dated tuff horizon in FAR-DEEP drill hole 8B from the Kolosjoki Sedimentary

326   Formation is interpreted as an eruption age, syn-depositional with sedimentation, and thus the

327   2056.6 ± 0.8 Ma age directly constrains the age at this stratigraphic level. Rocks immediately

328   under and overlying sample 8B 151.42m record normal $\delta^{13}C$ values (Fig. S4) and overlie the

329   Kuetsjärvi Sedimentary Formation (separated by the Kuetsjärvi Volcanic Formation; Fig. 4)

330   that bears the Lomagundi-Jatuli anomalous carbon isotope signature. The obtained age,

331   therefore, dates the termination of the Lomagundi-Jatuli Event. This date overlaps, within

332   uncertainty, with the c. 2055 to 2060 Ma detrital zircon dates (Il'mozero and Kolosjoki

333   Sedimentary Formation; Fig. 6b, c) that are inferred to closely approximate the timing of

334   broadly contemporaneous (Umba) volcanism. The Kolosjoki Sedimentary and Il'mozero

335   Sedimentary formations have long been considered as litho- and chemo-stratigraphic

336   equivalents (e.g. Melezhik and Sturt, 1994). The new age data confirm that they are also

337   chronostratigraphic equivalents, strengthening correlations between the two units. The new

338   carbon isotope data (Table 3) are consistent with existing data from the Il'mozero

339   Sedimentary Formation showing $\delta^{13}C$ values between -0.8 and +2.4‰ (Melezhik and Fallick,

340   1996) and signal a return to normal $\delta^{13}C$ values following the Lomagundi-Jatuli Event.

341

342   In Fennoscandia, the duration of the Lomagundi-Jatuli Event was first defined as 2200 –

343   2060 Ma (Karhu, 1993) and a termination age of 2050 ± 8 Ma (zircon; ID-TIMS) was

344   inferred based on felsic volcanic rocks associated with carbonate rocks having normal $\delta^{13}C$

345   values at the top of the Peräphoja Belt on the Karelia craton (Perttunen and Vaasjoki, 2001).

346   This overlaps, within uncertainty, with the 2056.6 ± 0.8 Ma age on the North

347   Transfennoscandian Greenstone Belt on the Kola craton. Initially, the Lomagundi-Jatuli

348   Event was thought to have continued at least until 2078 ± 8 Ma on Fennoscandia, based upon

349   ID-TIMS data from titanite and zircon fractions on an intrusive sill in the Kuusamo Schist

350   Belt (zircon and titanite fractions; ID-TIMS; Silvennoinen, 1991). Utilising this constraint,

351   the termination of the Lomagundi-Jatuli Event on Fennoscandia could be constrained to

352   between 2078 ± 8 and 2056.6 ± 0.8 Ma. However, the primary nature of the dated titanite

353   fractions that provide this constraint have recently been called into question (Hanski et al.,

354   2001). If this is accepted, then the next closest age constraints are c. 2200 Ma (e.g. Perttunen,

355   1991; Perttunen & Vaasjoki 2001; Silvennoinen, 1991).

356

357   Units recording the Lomagundi-Jatuli Event crop out in the Silverton Formation of the

358   Transvaal Supergroup in South Africa, with $\delta^{13}C$ values between +2 and +10‰ (Frauenstein

359   et al., 2009). Stratigraphically overlying the Silverton Formation, carbonate rocks in the

360   Houtenbek Formation record a return to normal $\delta^{13}C$ values between -3.3 and -0.5‰

361   (Melezhik and Fallick, 2010, and references therein). Above this formation (and separated by

362   the Dullstroom lava), the intrusions of the Bushveld Complex yield zircons dated by the U-Pb

363   ID-TIMS technique at 2054 ± 2 Ma (Scoates and Friedman, 2008), providing a minimum age

364   for the termination of the Lomagundi-Jatuli Event in the Transvaal Basin. Thus, age

365   constraints for the termination of the Lomagundi-Jatuli Event overlap, within uncertainty,

366   between Fennoscandia (2056.6 ± 0.8 Ma, North Transfennoscandian Greenstone Belt; 2050 ±

367 8 Ma, Peräphoja Schist Belt) and South Africa (2054 ± 2 Ma, Transvaal Basin). The

368 focussing of radio-isotopic age constraints on the transition from positive to normal δ^{13}C

369 values at c. 2060 Ma is also suggestive of global synchronism.

370

371 7. Conclusions

372 The two largest and economically important segments of the North Transfennoscandian

373 Greenstone Belt in NW Russia (Pechenga and Imandra-Varzuga) can be correlated based

374 upon litho-, chemo-, and now chrono-stratigraphy, with radiometric ages at 2056.6 ± 0.8 Ma

375 (Kolosjoki Sedimentary Formation) and 2055.5 ± 2.3 Ma (Il'mozero Sedimentary

376 Formation). This complements the existing radiometric ages of 2058 ± 2 Ma and 2049 ± 28

377 Ma (Melezhik et al., 2007) from Pechenga. The termination of the Lomagundi-Jatuli Event in

378 the North Transfennoscandian Greenstone Belt, and Fennoscandia, can be confined to >

379 2056.6 ± 0.8 Ma. This overlaps with, within error, the termination of the Lomagundi-Jatuli

380 Event from the Transvaal Supergroup, South Africa, constrained at > 2054 ± 2 Ma (Scoates

381 and Friedman, 2008).

382

386

387 References

388 Aharon, P., 2005. Redox stratification and anoxia of the early Precambrian oceans:
389   Implications for carbon isotope excursions and oxidation events. Precambrian
390   Research 137, 207-222.
391 Alapieti, T.T., Lahtinen, J.J., 2002. Platinum-Group Element Mineralization in Layered
392   Intrusions of Northern Finland and the Kola Peninsula, Russia, in: Cabri, L.J. (Ed.),
393   The Geology, Geochemistry, Mineralogy and Mineral Benefication of Platinum-group
394   Elements. CIM Special Volume 54, pp. 507-546.
395 Amelin, Y.V., Heaman, L.M., Semenov, V.S., 1995. U-Pb geochronology of layered mafic
396   intrusions in the eastern Baltic Shield: implications for the timing and duration of
397   Paleoproterozoic continental rifting. Precambrian Research 75, 31-46.
398 Baker, A.J., Fallick, A.E., 1989. Evidence from Lewisian limestones for isotopically heavy
399   carbon in two-thousand-million-year old sea water. Nature 337, 352-354.
400 Boggs, S.J., 2010. Petrology of Sedimentary Rocks, 2nd ed. Cambridge University Press,
401   Cambridge.

402 Condon, D.J., Bowring, S.A., 2011. Chapter 9 A user's guide to Neoproterozoic
403   geochronology. Geological Society, London, Memoirs 36, 135-149.
404 Condon, D.J., McClean, N., Noble, S.R., Bowring, S.A., 2010. Isotopic composition
405   ($^{238}U/^{235}U$) of some commonly used uranium reference materials. Geochimica et
406   Cosmochimica Acta 74, 7127-7143.
407 Frauenstein, F., Veizer, J., Beukes, N., Van Niekerk, H.S., Coetzee, L.L., 2009. Transvaal
408   Supergroup carbonates: Implications for Palaeoproterozoic $\delta^{18}O$ and $\delta^{13}C$ records.
409   Precambrian Research 175, 149-160.
410 Galimov, I.M., Kuznetsova, N.G., Prokhorov, V.S., 1968. The problem of the composition of
411   the Earth's ancient atmosphere in connection with results of isotopic analyses of
412   carbon from Precambrian carbonates. Geochemistry 11, 1376-1381 (in Russian).
413 Hanski, E.J., Huhma, H., Smol'kin, V.F., Vaasjoki, M., 1990. The age of ferropicritic
414   volcanites and comagmatic Ni-bearing intrusions at Pechenga, Kola Peninsula,
415   U.S.S.R. Geological Survey of Finland Bulletin 62, 123-133.
416 Hanski, E.J., Huhma, H., Vaasjoki, M., 2001. Geochronology of northern Finland: A
417   summary and discussion. Geological Survey of Finland, Special Paper 33, 255-279.
418 Hiess, J., Condon, D.J., McClean, N., Noble, S.R., 2012. $^{238}U/^{235}U$ systematics in terrestrial
419   U-bearing minerals. Science 335, 1610-1614.
420 Jaffey, A.H., Flynn, K.F., Glendenin, L.E., Bentley, W.C., Essling, A.M., 1971. Precision
421   measurement of half-lives and specific activities of ^{235}U and ^{238}U. Physics Reviews,
422   C4, 1889-1906.
423 Karhu, J.A., 1993. Palaeoproterozoic evolution of the carbon isotope ratios of sedimentary
424   carbonates in the Fennoscandian Shield. Geological Survey of Finland Bulletin 371,
425   1-87.
426 Karhu, J.A., Holland, H.D., 1996. Carbon isotopes and the rise of atmospheric oxygen.
427   Geology 24, 867-870.
428 Kozlovsky, Y.A., 1987. The Superdeep Well of the Kola Peninsula. Spinger Verlag, Berlin,
429   p. 558.
430 Mattinson, J.M., 2005. Zircon U-Pb chemical abrasion ("CA-TIMS") method: Combined
431   annealing and multi-step partial dissolution analysis for improved precision and
432   accuracy of zircon ages. Chemical Geology 220, 47-66.
433 Melezhik, V., Prave, A., Fallick, A., Hanski, E., Lepland, A., Kump, L., Strauss, H., 2012a.
434   Reading the Archive of Earth's Oxygenation. Springer, Heidelberg (in press).
435 Melezhik, V.A., Fallick, A.E., 1996. A widespread positive $\delta^{13}C$ carb anomaly at around
436   2.33-2.06 Ga on the Fennoscandian Shield: a paradox? Terra Nova 8, 141-157.
437 Melezhik, V.A., Fallick, A.E., 2010. On the Lomagundi-Jatuli carbon isotopic event: The
438   evidence from the Kalix Greenstone Belt, Sweden. Precambrian Research 179, 165-
439   190.
440 Melezhik, V.A., Fallick, A.E., Hanski, E., Kump, L., Lepland, A., Prave, A., Strauss, H.,
441   2005. Emergence of the aerobic biosphere during the Archean-Proterozoic transition:
442   Challenges for future research. Geological Society of America Today 15, 4-11.
443 Melezhik, V.A., Fallick, A.E., Martin, A.P., Condon, D.J., Kump, L.R., Brasier, A.T.,
444   Salminen, P., 2012b. The greatest perturbation of the global carbon cycle: the
445   Lomagundi-Jatuli isotopic event, in: Melezhik, V., Prave, A., Fallick, A., Hanski, E.,
446   Lepland, A., Kump, L., Strauss, H. (Eds.), Reading the Archive of Earth's
447   Oxygenation. Volume 2: The Core Archive of the Fennoscandian Arctic Russia-
448   Drilling Early Earth Project. Springer, Heidelberg (in press).
449 Melezhik, V.A., Huhma, H., Condon, D.J., Fallick, A.E., Whitehouse, M.J., 2007. Temporal
450   constraints on the Paleoproterozoic Lomagundi-Jatuli carbon isotopic event. Geology
451   35, 655-658.

452   Melezhik, V.A., Prave, A.R., Lepland, A., Hanski, E.J., Romashkin, A.E., Rychanchik, D.V.,
453   Luo, Z.-Y., 2012c. Kuetsjärvi Sedimentary Formation: FAR-DEEP Hole 5A,
454   neighbouring quarry and related outcrops, in: Melezhik, V., Prave, A., Fallick, A.,
455   Hanski, E., Lepland, A., Kump, L., Strauss, H. (Eds.), Reading the Archive of Earth's
456   Oxygenation. Volume 2: The Core Archive of the Fennoscandian Arctic Russia-
457   Drilling Early Earth Project. Springer, Heidelberg (in press).
458   Melezhik, V.A., Sturt, B.A., 1994. General geology and evolutionary history of the early
459   Proterozoic Polmak-Pasvik-Pechenga-Imandra/Varzuga-Ust'Ponoy Greenstone Belt
460   in the northeastern Baltic Shield. Earth-Science Reviews 36, 181-204.
461   Perttunen, V., Vaasjoki, M., 2001. U-Pb geochronology of the Perapohja schist belt,
462   northwestern Finland. Special Paper Geological Survey of Finland 33, 45-84.
463   Pettijohn, F.J., Potter, P.E., Siever, R., 1987. Sand and Sandstone, 2nd ed. Springer-Verlag,
464   New York.
465   Schidlowski, M., Eichmann, R., Junge, C.E., 1975. Precambrian sedimentary carbonates:
466   carbon and oxygen isotope geochemistry and implications for the terrestrial oxygen
467   budget. Precambrian Research 2, 1-69.
468   Schidlowski, M., Eichmann, R., Junge, C.E., 1976. Carbon isotope geochemistry of the
469   Precambrian Lomagundi carbonate province, Rhodesia. Geochimica et Cosmochimica
470   Acta 40, 449-455.
471   Scoates, J.S., Friedman, R.M., 2008. Precise age of the platiniferous Merensky Reef,
472   Bushveld Complex, South Africa, by the U-Pb zircon chemical abrasion ID-TIMS
473   technique. Economic Geology and the Bulletin of the Society of Economic Geologists
474   103, 465-471.
475   Sharkov, E.V., Smolkin, V.F., 1997. The early Proterozoic Pechenga-Varzuga Belt: a case of
476   Precambrian back-arc spreading. Precambrian Research 82, 133-151.
477   Shields, G.A., Veizer, J., 2002. The Precambrian marine carbonate isotope database: version
478   1.1. Geochemistry, Geophysics, Geosystems 3, 10.1029/2001GC000266.
479   Silvennoinen, A., 1991. Kuusamon ja Rukatunturin kartta-alueiden kallioperä. Summary:
480   Pre-Quaternary rocks of the Kuusamo and Rukatunturi map-sheet areas. Explanation
481   to the maps of Pre-Quaternary rocks, sheets 4524+4542. Geological map of Finland
482   1:100,000, 63 p.
483   Stirling, C.H., Andersen, M.B., Potter, E.K., Halliday, A.N., 2007. Low-temperature isotopic
484   fractionation of uranium. Earth and Planetary Science Letters 264, 208-225.
485   White, J.D.L., Houghton, B.F., 2006. Primary Volcaniclastic Rocks. Geology 34, 677-680.
486
487

488 **Figure 1.** Location of the segments of the North Transfennoscandian Greenstone Belt.

489
490
491
492
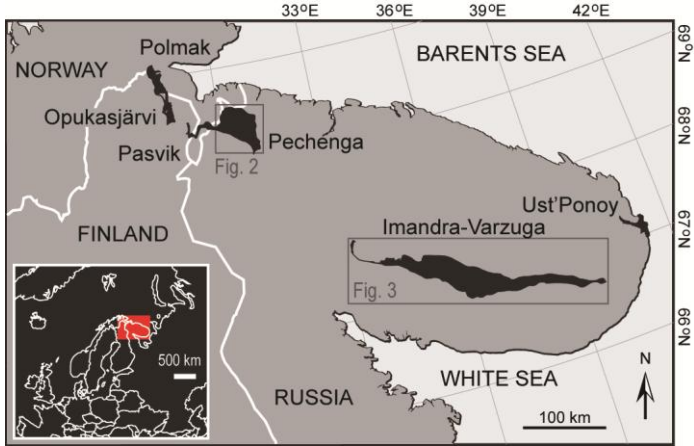
Figure. 2. The Pechenga Greenstone Belt after Melezhik and Sturt (1994). See the text for a description of the units and Fig. 4 for the stratigraphic column.
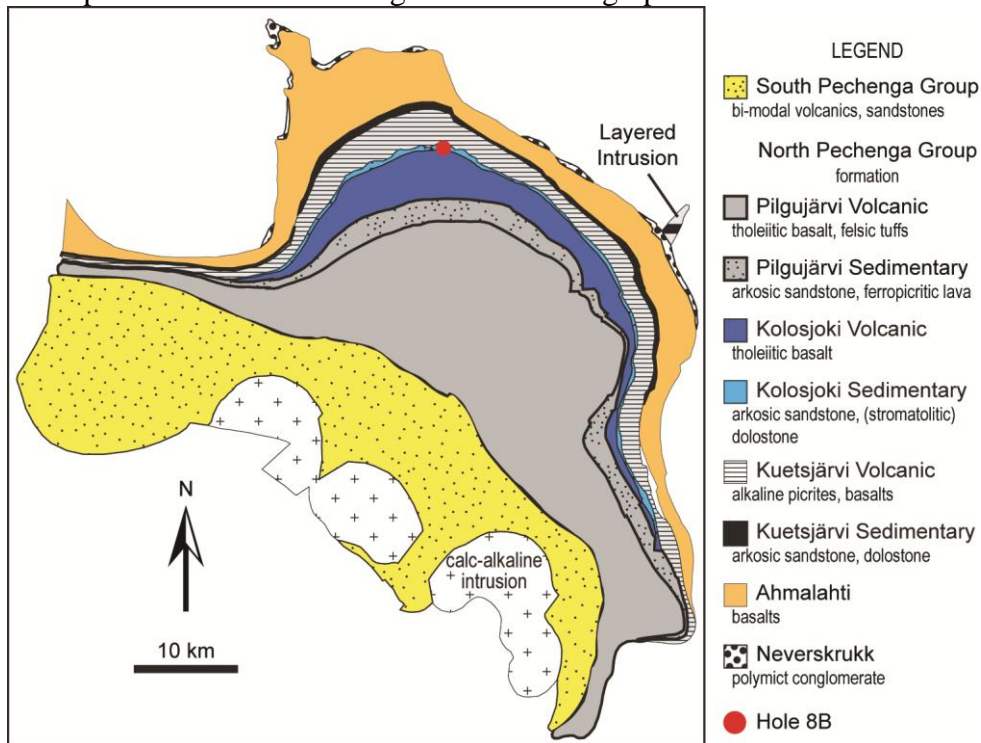
497 **Figure 3.** The Imandra-Varzuga Greenstone Belt after Melezhik and Sturt (1994). See the
498 text for a description of the units and Fig. 4 for the stratigraphic column.

LEGEND

Tominga Group
bi-modal volcanics, sandstones

Varzuga / Strelna Group
formation

Il'mozero Volcanic
basaltic andesites, dacites

Il'mozero Sedimentary
greywacke, dolostone

Umba Volcanic
alkaline picrites, trachybasalts

U Umba Sedimentary
quartzitic sandstone, dolostone

Polisarka Volcanic
komatiitic basalt, basaltic andesite

Polisarka Sedimentary
polymict conglomerate, greywacke, diamictite

Seidorechka Volcanic
Komatiitic basalt, basaltic andesite, dacite, rhyolite

Seidorechka Sedimentary
arkosic sandstone, greywacke-shale, dolostone

Kuksha Volcanic
tholeiitic basalt

Kuksha Sedimentary
greywacke, arkosic sandstone

Purnach
polymict sandstone, tholeiitic basalt

● Sample locality

499
500

501 **Figure. 4.** Stratigraphic columns after Melezhik and Sturt (1994) of a. The Pechenga
502 Greenstone Belt, and b. The Imandra-Varzuga Greenstone Belt. The new radiometric dates
503 (this study) are boxed. Published, relevant ages are from: 1. Hanski et al. (1990); 2. Melezhik
504 et al. (2007); 3. Amelin et al. (1995). R = rhyolite (granite); D = dacite (granodiorite); A =
505 andesite (diorite); B = basalt (gabbro); P = picrite (ultramafic). The patterns used for
506 formations in the stratigraphic columns match those used for formations in Fig. 2 and 3. The
507 values in the Group column are maximum reported $\delta^{13}C$ values (‰ V-PDB) for the adjacent
508 formation, taken from: A: (Melezhik et al., 2007); B. (Melezhik and Fallick, 1996Melezhik
509 and Fallick, 1996).
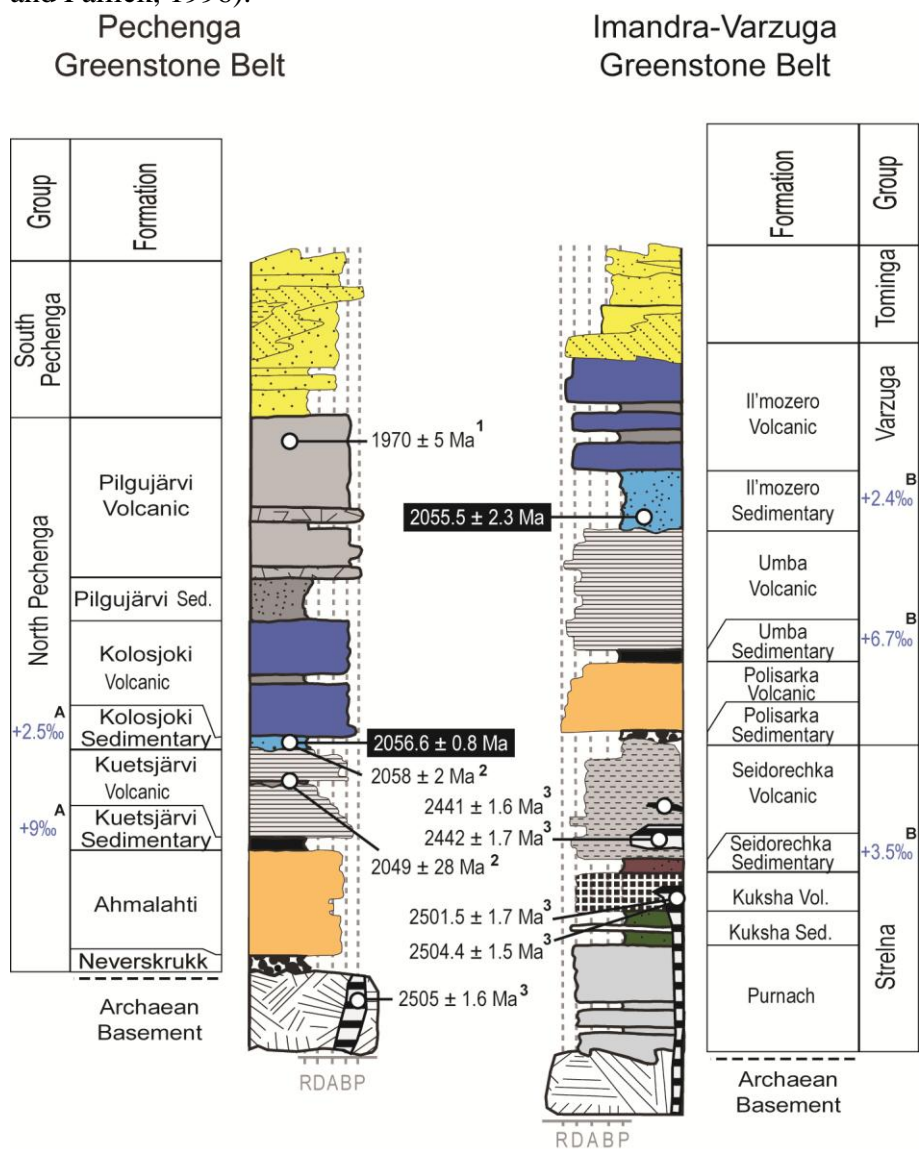
510
511

512 **Figure 5.** Petrography of dated samples. a. Il'mozero 1 in thin section. b. A scanned image
513 of Sample 8B 151.42m in hand specimen. Fragments of pumice, crystals (feldspar), and rare
514 jasper are visible.
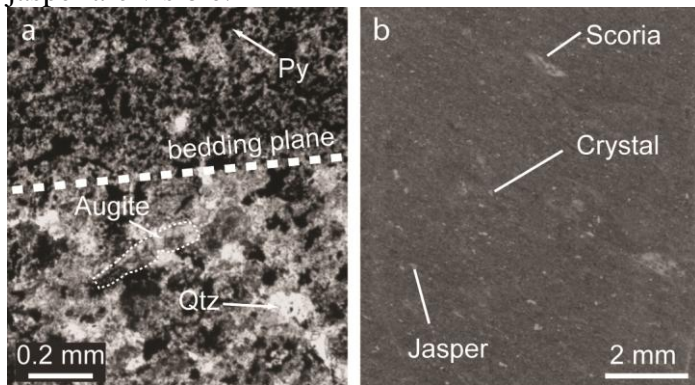
515
516

517   **Figure 6.** a. Conventional concordia plot for zircons from samples Il'mozero 1 (Imandra-
518   Varzuga) and 8B 151.42m (Pechenga) for single zircon grains analysed by the ID-TIMS
519   method. The data from Melezhik et al. (2007) from single zircon grains from the Kolosjoki
520   Sedimentary Formation (from Pechenga and the same formation as sample 8B 151.42m) are
521   included for comparison. b. ^{207}Pb-^{206}Pb plot of data from Fig. 6a.

522
523
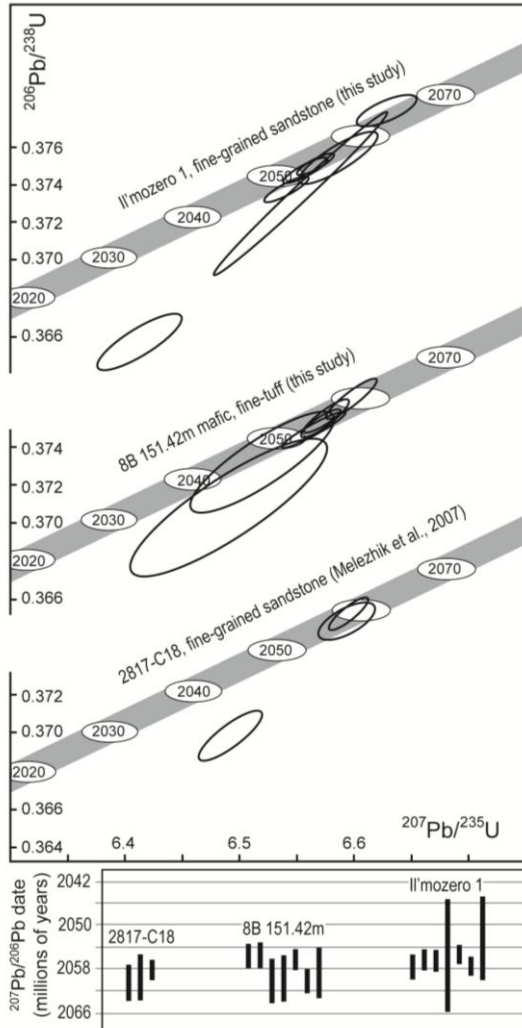
524 **Table 1** Zircon U-Pb LA-ICPMS data for sample Il'mozero 1.

Zr	Signals						Ratios									Isotopic ages						
	^{204}Pb (cps)	^{206}Pb (mV)	^{207}Pb (mV)	^{238}U (mV)	Pb (ppm)	U (ppm)	^{238}U/^{206}Pb	1σ %	^{207}Pb/^{206}Pb	1σ %	^{207}Pb/^{235}U	1σ %	^{206}Pb/^{238}U	1σ %	Rho	^{207}Pb/^{206}Pb	2σ abs	^{206}Pb/^{238}U	2σ abs	^{207}Pb/^{235}U	2σ abs	% conc.
1	18	3.0	0.7	8.2	74	124	1.71	1.01	0.2405	0.50	19.3866	1.13	0.5846	1.01	0.90	3123.4	8.0	2967.4	48.1	3061.3	21.6	95.0
3	231	2.6	0.5	8.0	63	121	1.93	1.21	0.1984	1.10	14.1409	1.64	0.5169	1.21	0.74	2813.2	17.9	2686.0	53.2	2759.2	30.6	95.5
6	126	5.8	1.0	17.7	142	269	1.96	1.36	0.1948	0.50	13.6830	1.45	0.5094	1.36	0.94	2783.4	8.2	2653.9	58.9	2728.0	27.1	95.3
10	-227	10.9	1.3	46.3	265	704	2.73	1.26	0.1284	0.50	6.4800	1.36	0.3659	1.26	0.93	2076.6	8.8	2010.2	43.4	2043.2	23.6	96.8
14	187	4.4	1.0	11.3	106	172	1.64	0.88	0.2426	0.50	20.3781	1.01	0.6093	0.88	0.87	3136.8	7.9	3067.3	42.6	3109.5	19.3	97.8
15	71	3.0	0.4	12.9	73	196	2.74	0.93	0.1290	0.50	6.4957	1.05	0.3651	0.93	0.88	2084.9	8.8	2006.3	31.9	2045.3	18.4	96.2
17	142	10.8	1.3	46.5	264	707	2.72	0.90	0.1301	0.50	6.5944	1.03	0.3677	0.90	0.87	2098.9	8.8	2018.6	31.1	2058.6	18.0	96.2
18	-90	3.7	0.4	15.5	90	236	2.66	0.96	0.1284	0.50	6.6677	1.08	0.3766	0.96	0.89	2076.3	8.8	2060.4	33.8	2068.3	19.0	99.2
19	-70	2.1	0.5	5.0	51	76	1.52	0.97	0.2750	0.50	24.9618	1.09	0.6584	0.97	0.89	3334.6	7.8	3260.9	49.6	3306.7	21.1	97.8
20	101	8.1	1.4	24.3	197	370	1.90	1.35	0.1880	0.50	13.6164	1.44	0.5252	1.35	0.94	2725.2	8.2	2721.0	59.6	2723.4	26.8	99.8
21	139	11.6	1.4	49.0	283	746	2.69	1.01	0.1294	0.50	6.6366	1.13	0.3719	1.01	0.90	2090.3	8.8	2038.2	35.3	2064.2	19.7	97.5
22	65	12.3	1.4	50.6	300	770	2.67	1.13	0.1280	0.50	6.6054	1.24	0.3743	1.13	0.91	2070.3	8.8	2049.8	39.6	2060.1	21.6	99.0
23	-69	7.2	0.8	30.5	174	464	2.72	0.94	0.1277	0.50	6.4748	1.06	0.3677	0.94	0.88	2066.9	8.8	2018.4	32.5	2042.5	18.6	97.7
24	45	7.0	1.0	24.4	170	371	2.22	0.98	0.1606	0.50	9.9750	1.10	0.4505	0.98	0.89	2461.7	8.4	2397.7	39.3	2432.5	20.2	97.4
26	-36	3.0	0.4	13.0	74	197	2.73	1.03	0.1295	0.52	6.5444	1.16	0.3666	1.03	0.89	2090.7	9.2	2013.5	35.7	2051.9	20.2	96.3
27	153	5.6	0.6	23.7	135	360	2.72	0.94	0.1276	0.50	6.4708	1.06	0.3678	0.94	0.88	2065.1	8.8	2019.1	32.5	2041.9	18.6	97.8
28	310	2.0	0.2	8.5	48	130	2.77	1.01	0.1292	0.50	6.4351	1.12	0.3613	1.01	0.90	2086.7	8.8	1988.5	34.4	2037.1	19.6	95.3
29	241	21.2	6.7	45.5	516	692	1.36	0.94	0.3469	0.50	35.0611	1.07	0.7331	0.94	0.88	3693.4	7.6	3544.8	51.1	3640.4	20.8	96.0
30	184	13.8	1.6	58.5	337	890	2.74	1.07	0.1279	0.50	6.4380	1.18	0.3649	1.07	0.91	2069.9	8.8	2005.5	36.8	2037.5	20.6	96.9
31	126	11.7	2.8	28.5	285	433	1.57	1.01	0.2606	0.50	22.9629	1.13	0.6390	1.01	0.90	3250.6	7.9	3185.0	50.5	3225.4	21.7	98.0
32	79	5.7	0.7	24.1	139	366	2.70	0.92	0.1274	0.50	6.5192	1.05	0.3710	0.92	0.88	2063.0	8.8	2034.1	32.2	2048.5	18.3	98.6
33	613	21.5	2.6	90.5	523	1377	2.67	1.01	0.1341	1.29	6.9126	1.63	0.3739	1.01	0.62	2152.2	22.4	2047.6	35.3	2100.3	28.6	95.1
34	69	5.4	0.6	23.6	132	359	2.76	1.11	0.1280	0.50	6.3964	1.22	0.3623	1.11	0.91	2071.1	8.8	1993.2	38.0	2031.8	21.2	96.2
35	-186	9.1	1.7	25.9	221	395	1.82	0.91	0.2090	0.50	15.8551	1.04	0.5503	0.91	0.88	2897.6	8.1	2826.3	41.5	2868.1	19.6	97.5
36	-233	5.0	0.8	16.4	121	249	2.09	0.95	0.1766	0.50	11.6675	1.08	0.4792	0.95	0.89	2621.2	8.3	2523.6	39.7	2578.1	19.9	96.3
37	189	10.3	1.2	43.3	251	659	2.58	2.01	0.1345	0.98	7.1840	2.24	0.3874	2.01	0.90	2157.6	17.2	2110.6	72.1	2134.5	39.2	97.8

40	-54	4.7	0.5	21.2	116	323	2.85	0.90	0.1233	0.50	5.9554	1.03	0.3504	0.90	0.87	2003.8	8.9	1936.7	29.9	1969.4	17.7	96.6
41	-102	6.5	0.8	27.0	158	411	2.65	0.86	0.1320	0.50	6.8715	1.00	0.3775	0.86	0.87	2124.9	8.8	2064.6	30.4	2095.0	17.5	97.2
46	-247	7.9	0.9	33.4	192	509	2.71	0.97	0.1279	0.50	6.5066	1.09	0.3688	0.97	0.89	2069.9	8.8	2023.9	33.5	2046.8	19.0	97.8
47	-239	8.4	1.0	35.8	204	544	2.68	1.08	0.1297	0.50	6.6694	1.19	0.3728	1.08	0.91	2094.6	8.8	2042.6	37.6	2068.6	20.8	97.5
51	-56	9.7	1.7	29.7	238	452	1.94	1.01	0.1925	0.50	13.6591	1.13	0.5145	1.01	0.90	2764.0	8.2	2675.8	44.1	2726.4	21.1	96.8
52	-73	1.0	0.2	2.8	24	43	1.79	0.88	0.2205	0.59	16.9648	1.06	0.5579	0.88	0.83	2984.5	9.5	2858.1	40.6	2932.8	20.2	95.8
58	34	7.6	0.9	32.8	185	499	2.73	1.03	0.1299	0.50	6.5547	1.15	0.3660	1.03	0.90	2096.5	8.8	2010.5	35.6	2053.3	20.0	95.9
59	130	19.1	2.3	81.9	464	1246	2.72	0.86	0.1297	0.50	6.5727	0.99	0.3675	0.86	0.86	2094.1	8.8	2017.6	29.6	2055.7	17.3	96.3
60	-66	13.5	1.6	57.5	328	875	2.71	0.90	0.1283	0.50	6.5309	1.03	0.3692	0.90	0.87	2074.8	8.8	2025.6	31.2	2050.1	18.0	97.6

525
526

Table 2   U-Th-Pb data for zircons analysed by ID-TIMS from samples Il'mozero 1. and 8B 151.42m.

Fraction	$\frac{\text{Th}}{\text{U}}$	^{206}Pb* x10^{-13} mol	mol % ^{206}Pb*	$\frac{\text{Pb*}}{\text{Pb}_c}$	Pb$_c$ (pg)	$\frac{^{206}\text{Pb}}{^{204}\text{Pb}}$	$\frac{^{208}\text{Pb}}{^{206}\text{Pb}}$	$\frac{^{207}\text{Pb}}{^{206}\text{Pb}}$	% err	$\frac{^{207}\text{Pb}}{^{235}\text{U}}$	% err	$\frac{^{206}\text{Pb}}{^{238}\text{U}}$	% err	corr. coef.	$\frac{^{207}\text{Pb}}{^{206}\text{Pb}}$	±	$\frac{^{207}\text{Pb}}{^{235}\text{U}}$	±	$\frac{^{206}\text{Pb}}{^{238}\text{U}}$	±
(a)	(b)	(c)	(c)	(c)	(c)	(d)	(e)	(e)	(f)	(e)	(f)	(e)	(f)		(g)	(f)	(g)	(f)	(g)	(f)
Il'mozero 1.																				
z1	0.786	1.1112	96.92%	11	2.92	592	0.229	0.127137	0.268	6.409819	0.472	0.365655	0.328	0.834	2058.70	4.74	2033.62	4.15	2008.98	5.66
z2	0.721	1.6171	98.88%	29	1.52	1627	0.208	0.127245	0.128	6.552413	0.955	0.373474	0.936	0.991	2060.19	2.25	2052.97	8.41	2045.79	16.41
z4	0.890	2.2009	99.17%	41	1.52	2196	0.256	0.126964	0.107	6.565059	0.208	0.375021	0.123	0.915	2056.30	1.89	2054.67	1.83	2053.04	2.17
z5	0.556	3.9797	93.30%	4	24.04	263	0.160	0.127131	0.404	6.568396	0.754	0.374718	0.539	0.856	2058.62	7.13	2055.12	6.64	2051.63	9.47
z6	0.668	1.0618	97.09%	11	2.64	625	0.192	0.127246	0.232	6.585170	0.428	0.375338	0.297	0.856	2060.21	4.10	2057.36	3.78	2054.53	5.22
z9	0.661	2.5597	99.05%	34	2.03	1924	0.190	0.126907	0.131	6.555718	0.228	0.374656	0.136	0.860	2055.50	2.31	2053.41	2.01	2051.33	2.39
z12	0.416	2.0918	98.66%	23	2.36	1354	0.120	0.126920	0.130	6.539981	0.248	0.373720	0.155	0.892	2055.67	2.30	2051.30	2.18	2046.95	2.72
8B 151.42m																				
z7	1.102	0.7030	94.99%	6	3.30	313	0.316	0.126777	0.268	6.578309	0.388	0.376335	0.230	0.737	2053.70	4.74	2056.45	3.42	2059.19	4.05
z10	0.579	1.1636	99.42%	55	0.56	3154	0.166	0.127051	0.102	6.574262	0.207	0.375290	0.132	0.913	2057.51	1.79	2055.90	1.82	2054.31	2.32
z11	0.578	1.3082	99.37%	51	0.69	2890	0.166	0.126899	0.101	6.554642	0.223	0.374620	0.155	0.918	2055.38	1.78	2053.27	1.96	2051.17	2.73
z12	0.524	0.5316	93.06%	4	3.53	225	0.151	0.127043	0.322	6.575673	0.469	0.375394	0.289	0.738	2057.39	5.68	2056.09	4.14	2054.80	5.08
z20	0.721	1.5560	99.04%	33	1.30	1739	0.207	0.126989	0.103	6.575766	0.208	0.375560	0.128	0.921	2056.64	1.81	2056.10	1.83	2055.57	2.26
z21	0.548	0.7336	99.25%	43	0.46	2439	0.157	0.126969	0.109	6.575673	0.244	0.375614	0.177	0.914	2056.36	1.92	2056.09	2.15	2055.83	3.12
z24	0.469	0.5306	98.79%	26	0.54	1498	0.135	0.127062	0.129	6.596177	0.290	0.376510	0.218	0.908	2057.64	2.28	2058.84	2.56	2060.03	3.85

Radiogenic Isotope Ratios

Isotopic Ages

(a) z1, z2 etc. are labels for fractions composed of single zircon grains or fragments; all fractions annealed and chemically abraded after Mattinson (2005).

(b) Model Th/U ratio calculated from radiogenic ^{208}Pb/^{206}Pb ratio and ^{207}Pb/^{235}U age.

(c) Pb* and Pb$_c$ represent radiogenic and common Pb, respectively; mol % ^{206}Pb* with respect to radiogenic, blank and initial common Pb.

(d) Measured ratio corrected for spike and fractionation only.

(e) Corrected for fractionation, spike, and common Pb; up to 1 pg of common Pb was assumed to be procedural blank: ^{206}Pb/^{204}Pb = 18.20 ± 0.50%; ^{207}Pb/^{204}Pb = 15.65 ± 0.40%; ^{208}Pb/^{204}Pb = 38.20 ± 0.75% (all uncertainties 1-sigma). Excess over blank was assigned to initial common Pb.

(f) Errors are 2-sigma, propagated using the algorithms of Schmitz and Schoene (2007).

(g) Calculations are based on the decay constants of Jaffey et al. (1971). ^{206}Pb/^{238}U and ^{207}Pb/^{206}Pb ages corrected for initial disequilibrium in ^{230}Th/^{238}U using Th/U [magma] = 4.

^{206}Pb/^{238}U dates in bold are those used in the weighted mean zircon date calculation

532 **Table 3.** The $\delta^{13}C$ and $\delta^{18}O$ values from carbonate rocks in the Il'mozero Sedimentary
533 Formation (‰ relative to Vienna Pee Dee Belemnite and Standard Mean
534 Ocean Water).
535

sample	height (m)	$\delta^{13}C$ ‰	$\delta^{18}O$ ‰
ILM-1	0.5	-0.7	-13.8
ILM-2	1.0	1.5	-13.3
ILM-3	2.5	2.0	-12.0
ILM-4	3.5	2.2	-11.7
ILM-5	5.5	2.6	-10.9
ILM-6	7.0	2.5	-10.6
ILM-7	9.0	2.5	-9.3

536
537 Height (m) = the height in metres above the contact between the greywacke and first carbonate rock in the
538 Il'mozero Sedimentary Formation.
539
540